ACS APPLIED MATERIALS & INTERFACES

Research Article

www.acsami.org

Synthesis and Application of Photolithographically Patternable Deep Blue Emitting Poly(3,6-Dimethoxy-9,9-dialkylsilafluorene)s

Jeffrey J. McDowell,[†] Florian Maier-Flaig,[‡] Thomas J. A. Wolf,[#] Andreas-Neil Unterreiner,[#] Uli Lemmer,[‡] and Geoffrey Ozin*[,†]

[†]Department of Chemistry, University of Toronto, 80 St. George Street, Toronto, Ontario, M5S 3H6, Canada

[‡]Light Technology Institute (LTI), Karlsruhe Institute of Technology (KIT), Engesserstrasse 13, Building 30.34, 76131 Karlsruhe, Germany

[#]Institute of Physical Chemistry, Karlsruhe Institute of Technology (KIT), Kaiserstraße 12, 76131 Karlsruhe, Germany

Supporting Information

ABSTRACT: Poly(silafluorene)s (PSFs) are promising light-emitting materials with brilliant solid-state blue luminescence, high quantum efficiency, excellent solubility, and improved thermal and chemical stability. PSFs are reported to have high electron affinity and conductivity originating from $\sigma^*-\pi^*$ conjugation between the σ^*-antibonding orbital of the exocyclic Si−C bond and the π^* antibonding orbital of the butadiene fragment, a promising characteristic for improved charge carrier balance in OLEDs. In this paper, we present a protocol for photopatterning derivatives of poly(3,6-dimethoxy-9,9-dialkylsilafluorenes) with resolutions exceeding 10 μm. The procedure begins by converting polymers (M_n = 50−55 kg/mol, PDI = 1.8) with cyclohexenyl and norbornenyl containing side chains to their respective epoxides using the Prilezhaev reaction and *m*-chloroperoxybenzoic acid (m-CPBA). Using the I-line (365 nm) of a Karl Suss MA6 mask aligner, a 1 s UV light exposure of the photoacid generator (PAG) bis(4-*tert*-butylphenyl)iodonium hexafluoro-phosphate (DtBPI-PF_6) generates sufficient protons to catalyze epoxide ring-opening and form a bridging network of covalent C−O bonds which renders the material insoluble in developing solvents such as toluene or THF. The resultant cross-linked material possess characteristic blue photoluminescence with solid state quantum yields >80%. Polymer films have excellent transparency (with a measured $E_g \approx 3.0$ eV). Energy levels determined using cyclic voltammetry were −5.7 and −2.7 eV for HOMO and LUMO, respectively. Additionally, several device applications are demonstrated which incorporate cross-linked films. These include examples of solid state lasing in the region of 420−450 nm from cross-linked films on second order corrugated silica substrates (Λ = 200 nm). OLEDs were also prepared with a cross-linked emitting layer as part of a trilayer device which we report to have a maximum external quantum efficiency of 3.2% at 33 mA/cm^2 and a stable blue-violet emission with an electroluminescence maximum at 410 nm. Photopatternable PSF epoxides are also shown to be efficient hosts for Förster energy transfer and we provide examples of pattern layers incorporating small molecule emitters which emit in both the red and green while blue emission of the host is effectively suppressed.

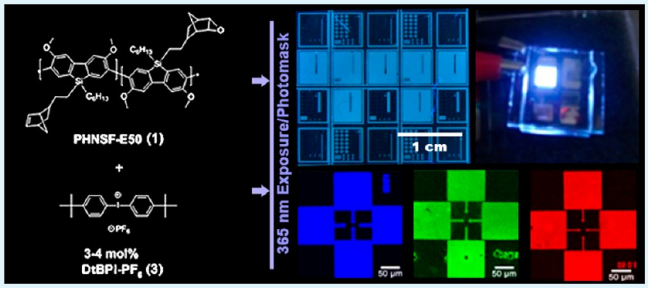

KEYWORDS: *conjugated polymer, light-emitting, photolithography, polymer light-emitting diode, polymer laser, polysilafluorene*

INTRODUCTION

The increasing prevalence of organic electronics in modern society warrants continued development of technologies that efficiently store, process, and display information. Commercialization of emerging display technologies places special demand on material costs and processing.[1−4] Polymer-based light emitting diodes are often considered low cost alternatives to their small molecule counterparts given the ease in which solutions can be made into thin films over relatively large areas without need for energy intensive high vacuum evaporation.[5−8] While the formation of contiguous thin films is paramount to the creation of emissive layers in simple organic light sources, other design consideration must be addressed in more advanced technologies. Polychromic displays require creation of addressable subpixels consisting of at least one of each primary color (red, green, blue, or RGB) and the resolution of the ensemble must be high enough to render an image amicable to the human eye (<50 μm). In modern active-matrix light emitting diode (AMOLED) devices, this is done by sequential vacuum evaporation of RGB emitters (through shadow masks) onto an array of transparent conductive electrodes (that is, indium-doped tin oxide (ITO)), which are powered by a thin-film transistor (TFT) backplane.[9] One method of shifting the AMOLED fabrication paradigm from vacuum to solution

Received: July 1, 2013
Accepted: September 11, 2013
Published: September 11, 2013

   dx.doi.org/10.1021/am4025406 | ACS Appl. Mater. Interfaces 2014, 6, 83−93

processing is through the invention of conjugated light emitting polymers, which serve the dual purpose of patternability and electroluminescence.

In this paper, we attempt to address some of the challenges in designing polymers suitable for creating pixelated polymer-based displays while utilizing protocols, which can easily integrate such materials into existing microfabrication methods. We show that poly(silafluorene) (PSF) derivatives synthesized as part of this work are promising candidates, which can not only be patterned with resolution <50 μm but also are produced using a simplified route involving fewer synthetic steps than the prior art (Figure 1a–d).[10,11] Epoxidized polymers poly(3,6-dimethoxy-9-hexyl-9-[2-(bicyclohept-5-en-2-yl)ethyl]silafluorene)(PHNSF-E50) (**1**) and poly(3,6-dimethoxy-9-hexyl-9-[2-(cyclohex-3-en-1-yl)ethyl]-silafluorene)-(PHCySF-E50) (**2**) (see Figure 1e) possess narrow solid state photoluminescence in the deep blue, can host numerous higher wavelength emitters, and can be processed into thin cross-linked films which electroluminesce under an applied voltage.

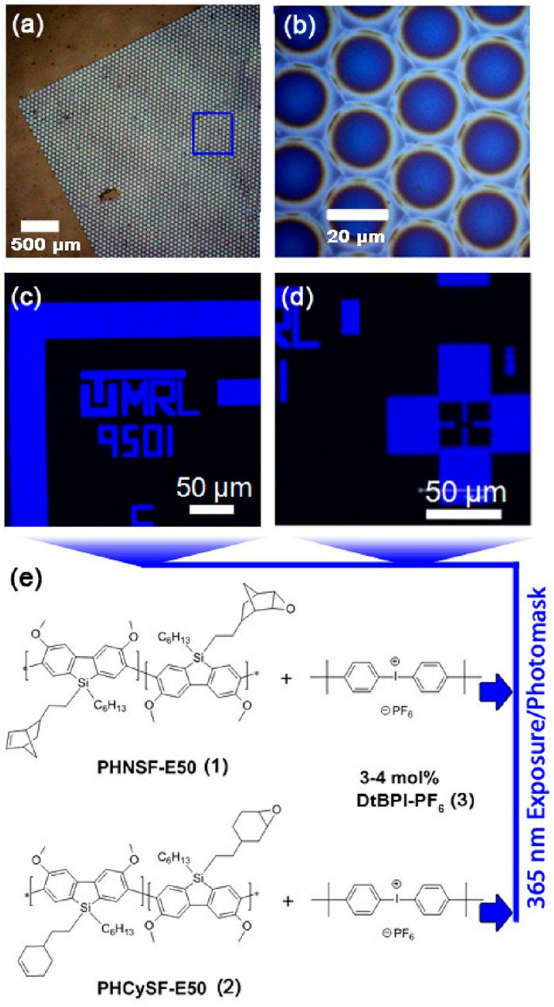

Figure 1. Conventional microscope images (a, b) and confocal fluorescent microscope images (c, d) of patterned films of PHNSF-E50 (**1**) and PHCySF-E50 (**2**), respectively. The low magnification image (a) demonstrates the high degree of fidelity of a patterned film to the original shadow mask. The blue highlighted area in panel a is magnified in panel b to better illustrate the hexagonally packed microdisk array. Panel e illustrates the structure of both photo-patternable polymers developed in this study (note the presence of epoxide groups on each polymer's side chains). The source of catalytic protons is the photoacid generator DtBPI-PF_6, which initiate the cross-linking following momentary exposure to UV light.

Our work is motivated by the seminal papers of Meerholz et al. who popularized the concept of photopatterning conjugated polymers.[12−16] Unlike common negative photopatternable resists such as SU8 (which employ epoxide groups), Meerholtz et al. utilized oxetane side chains as their mode of cross-linking. Oxetane derivatives consist of a four member oxygen containing ring which possess less internal strain than its three member counterpart. Consequently, oxetanes are less reactive toward ring-opening, a fact exploited by Meerholtz in their production of poly(spirobifluorene-co-fluorene) derivatives via Suzuki coupling. It is doubtful that inadvertent ring-opening of epoxides could be prevented under the conditions required for Suzuki. The trade-off for using less reactive cross-linking groups is the potential for patterning to requiring longer exposure/baking time, higher bake temperatures or higher loading of photoacid generator (PAG).[17,18] The risk of over developing may be higher if cross-link density does not exceed a threshold amount. The later point imposes limitations on the expected resolution.[17,18] Oxetanes, however, are proven to be an effective cross-linking moiety in high resolution photo-patterning.[12−16]

The polymers **1** and **2** produced in this paper possess epoxide side chains that serve the dual purpose of reducing baking and UV light exposure time, while additionally exploiting alternative synthetic pathways for the installation of cross-linkable moieties. Our postpolymerization epoxidation facilitates the overall synthesis (reducing synthetic steps and reaction time), while simultaneously improving performance of the material. Scheme 1 illustrates the process by which our epoxide functionalized poly(silafluorene)s cross-link (via a ring-opening polymerization) in the presence of an acid catalyst.

Scheme 1. Mechanism of Cationic Ring-Opening Polymerization (ROP) of Norbornenyl Oxide Side Chains on Polymer 1.[a]

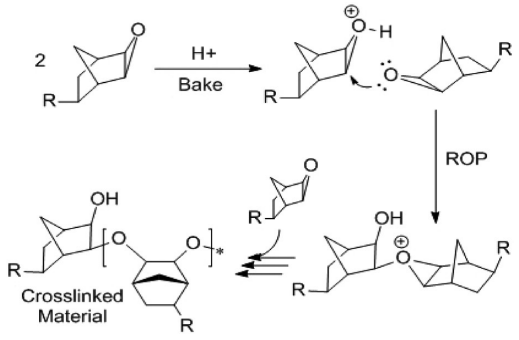

[a]Each R group represents a connection to a polymer backbone. Sufficient cross-links result in an insoluble material. The photoinduced decomposition of a PAG supplies a catalytic amount of acid which initiates the ROP.

Using the I-line (365 nm) of a Karl Suss MA6 mask aligner, a 1 s exposure of the photoacid generator (PAG) Bis(4-tert-butylphenyl)iodonium hexafluoro-phosphate (DtBPI-PF_6)(3) generates sufficient protons to catalyze epoxide ring-opening and form a bridging network of covalent C−O bonds which renders the material insoluble in developing solvents such as toluene or THF. This process was aided by a relatively low

dx.doi.org/10.1021/am4025406 | ACS Appl. Mater. Interfaces 2014, 6, 83−93

temperature soft bake at 90 °C. Following development, the smallest feature of our test pattern (10 μm) became visible (Figure 1). Photoluminescence of cross-linked areas exhibit no significant spectral changes or decline in quantum efficiency.

RESULTS AND DISCUSSION

We utilized an efficient nickel-catalyzed polymerization based on diarylmagnesate monomers to create poly(silafluorene)s PHCySF (**4**) and PHNSF (**5**) (Figures 2 and 3) in good yield

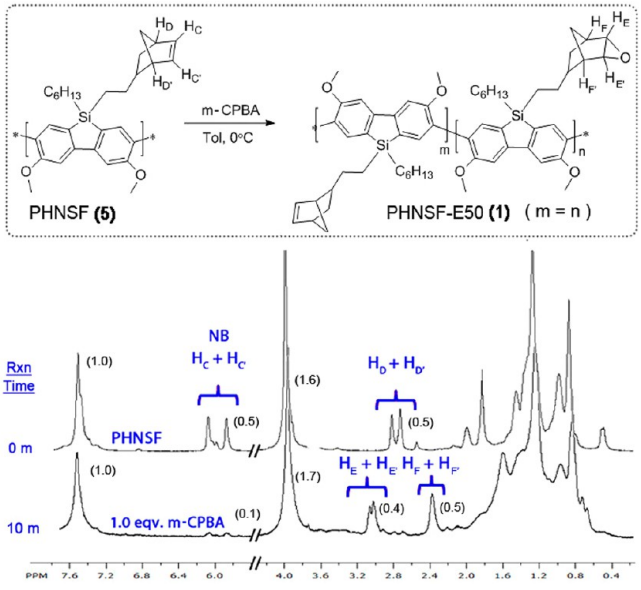

Figure 2. ^{1}H NMR confirms that m-CPBA oxidizes the strained double bonds of the PHNSF norbornenyl side groups without side reactions. In the presence of 1 equiv m-CPBA, alkenyl protons H_C/$H_{C'}$ (centered at 6.0 ppm) are ~80% converted to norbornenyl oxide protons H_E/$H_{E'}$ (centered at 2.7 ppm). Resonance peaks of neighboring norbornenyl protons H_D/$H_{D'}$ in PHNSF (at 2.6 ppm) are also observed to shift upfield during the conversion (corresponding H_F/$H_{F'}$ resonance peaks occur at 2.4 ppm) PHNSF (**5**) is a superior reagent for Prilezhaev epoxidation (vs PHCySF (**4**)) given the more complete oxidation of the norbornenyl double bond.

with number average molecular weights exceeding 50 kg/mol (See Supporting Information).[19] The polymerization was complete in less than 30 min and polymer was collected by simple precipitation in methanol. Excess monomer and oligomers were removed by subsequent Soxhlet extraction with ethanol over 5−6 h. Synthetically useful cycloalkenes, specifically cyclohexenyl (Cy) and norbornenyl (NB) moieties, are present in the side chain of each repeat unit of polymers **4** and **5**, respectively. In our previous publication, **4** and **5** were studied with regards to their solution and thin film absorption and photoluminescence properties.[19] Both polymers were found to have a large band gap, ~3 eV, and solution like optical properties in thin films indicative of its predominantly amorphous nature. We attribute the absence of microcrystalline phases to the methoxy groups located at the 3 and 6 positions on the repeat unit. For reasons of sterics, these groups are believed to impart a slight torsion to the backbone which prevents the occurrence of crystalline packing.[20] Referring to the absorption and photoluminescence spectra of polymers **4** and **5** in Figure 4c, the formation of microcrystalline phases leading to red-shifted and broadened emissions (such as the well documented β-phase formed in poly(9,9-dialkylfluorene)s)

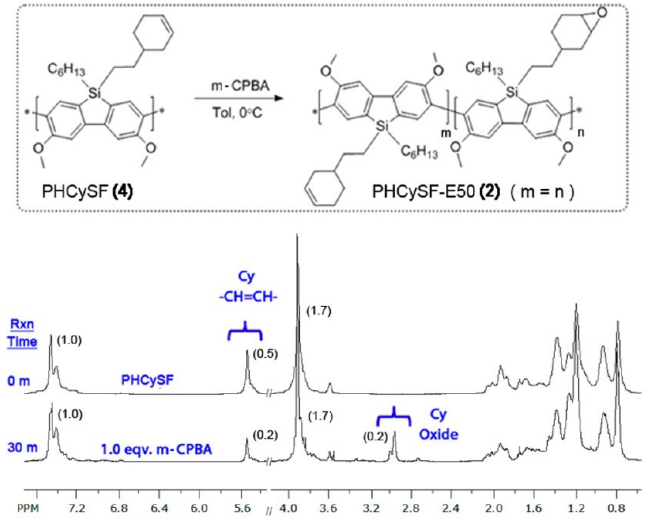

Figure 3. ^{1}H NMR taken during the Prilezhaev epoxidation of polymer **4** with m-CPBA. Note the maximum conversion of cyclohexenyl (Cy) side chains to their cyclohexenyl oxide (CyO) analogs was ~50% after 30 min (despite 1 equiv of m-CPBA having been added). CyO peaks at 3.0 ppm become apparent after several minutes of reaction while Cy peaks at 5.6 ppm simultaneously decreases. Peak integration is given in parentheses next to the corresponding peak.

are not observed.[21−24] Additionally, Figure 4c shows absorption and photoluminescence is essentially unchanged for thin films of polymer starting materials (PHCySF and PHNSF) and their epoxidized and cross-linked (XL) counterparts (PHCySF-E50 and PHNSF-E50). The unchanged position and shape of absorption and emission bands suggests that neither the epoxidation nor the photo-cross-linking procedure resulted in chemical alteration of the silafluorene emission center. Absolute quantum yields (AQY) of both cross-linked thin films also remains high at 86% and 83% for PHNSF-E50 and PHCySF-E50, respectively

In the interest of improving on the prior art, we deviated from the more synthetically complex process of oxetane functionalization (which would not have been compatible with our polymerization method) in favor of postpolymerization modification of the side-chain double bonds. Specifically, we employed the relatively simple process of converting the cycloalkene moiety into cycloalkene oxides using m-chloroperoxybenzoic acid (m-CPBA), for example, the Prilezhaev reaction.[25,26] This was accomplished via dropwise addition of m-CPBA/chloroform solution into a toluene solution of polymer cooled to 0 °C.

When conducting the reaction on an NMR scale using deuterated chloroform and toluene, the progress of the reaction was readily apparent from changes in the ^{1}H NMR as reaction time progressed (Figures 2 and 3). The norbornenyl moiety of polymer **5** was observed to be more reactive to epoxidation due in part to its higher internal strain energy relative to the nonbridged cyclohexenyl moiety.[27,28] Epoxidation was found to be rapid and high yielding (80−90% conversion) in the case of polymer **5** with a reagent molar ratio of [m-CPBA]/[NB] = 1 (figure 2). Norbornenyl protons resonance peaks centered at 6.0 ppm are replaced with those of norbornenyl oxide at 2.7 ppm. Furthermore, examination of aromatic proton resonance peaks in the region of 7.6−7.2 ppm suggests that oxidation is

dx.doi.org/10.1021/am4025406 | ACS Appl. Mater. Interfaces 2014, 6, 83−93

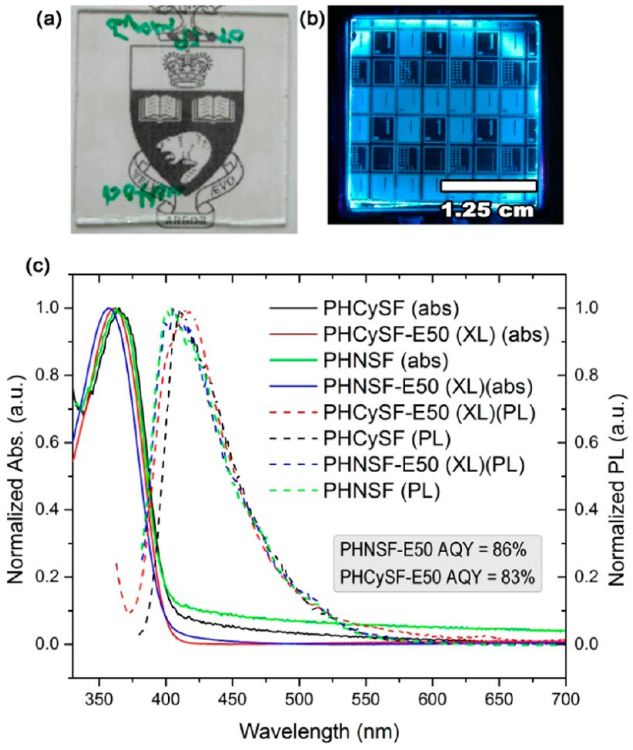

Figure 4. (a) Photograph of a transparent patterned film of PHNSF-E50 on glass. (b) Photograph of the same patterned film fluorescing under 365 nm illumination (with underlying printed logo removed). (c) Solid-state absorption (abs) and photoluminescence (PL) of polymer films. Note there is nearly complete overlap of absorption and PL spectra for thin films of polymer starting materials (PHCySF and PHNSF) and their epoxidized and cross-linked (XL) counterparts (PHCySF-E50 and PHNSF-E50). The unchanged position and shape of absorption and emission bands suggests that neither the epoxidation nor the photo-cross-linking procedure resulted in chemical alteration of the silafluorene repeat unit. Absolute quantum yields (AQY) of both cross-linked thin films was performed using an integrating sphere and measured to be 86% and 83% for PHNSF-E50 and PHCySF-E50, respectively.

regioselective for the cylcoalkene and undesirable oxidation of the polymer backbone remains undetectable by NMR.

In addition to complete epoxidation of polymer **5**, quantitative conversion of 50% and 25% of side chains is also possible by altering the equivalence of m-CPBA added. This tunability allows greater control over material properties such as cross-link density which can ultimately affect the resolution limit of developed features. Additionally, unreacted norbornenyl groups provide a handle for secondary side chain modification which may be useful in the installation of pendant emitters for tailoring electroluminescence.[29−32]

After the addition of m-CPBA to a solution of polymer **4** (with a reagent molar ratio of [m-CPBA]/[Cy] = 1), only approximately 50% for cyclohexenyl groups had oxidized to cyclohexenyl oxide after a period of 30 min. Looking at Figure 3, NMR shows the disappearance of alkene proton resonance at 5.6 ppm and the emergence of characteristic cyclohexene oxide peaks at 3.0 ppm.

For the purposes of photolithography in this paper, we limited of the conversion of cycloalkene side groups of polymers **4** and **5** to 50%. Purification of converted polymers, designated PHNSF-E50 (**1**) and PHCySF-E50 (**2**), is initiated by precipitating the product through the injection of hexanes into the reaction solution. The polymer is separated from the solvent, dried, and redissolved in the minimum amount of THF. Precipitation of polymer from THF into dry methanol a total of two times was sufficient to remove any traces of unreacted m-CPBA (and its reaction byproducts). Toluene solutions (16 mg/mL) of polymers **1** and **2** were subsequently made and stored with refrigeration until use.

Photolithography Methods. The generalized steps for producing a patterned surface are illustrated in Scheme 2.

Scheme 2. Procedural Diagram for Making Photopatterned Films of Polymers 1 and 2

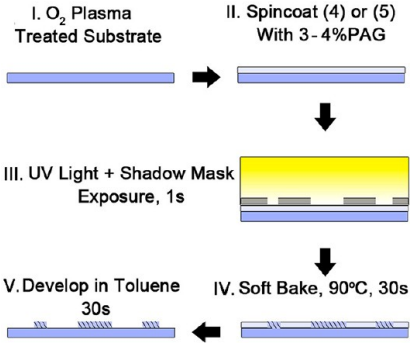

Optimum results with respect to highest AQY, minimal baking temperature, lowest PAG loading and highest resolution were obtained by using 16 mg/mL toluene solutions of polymers **1** and **2**. Polymer solutions were mixed 1:1 (v/v) with a 0.5 mg/mL DtBPI-PF_6 (in toluene) prior to use. For PHNSF-E50 and PHCySF-E50, this represents a 4 mol % loading of photoacid generator (with respect to epoxide groups). Spin-casting the mixed solution at 3000 rpm produces transparent, contiguous films with an average thickness of 80 nm, as determined by AFM (Veeco Dimension 3100). A short 1 s exposure to UV light through a shadow mask and a brief post bake step at 90 °C was used to create light emitting structures with resolvable features of <10 μm, Figure 4a and b.

Following UV exposure, the photoluminescence of irradiated areas was noticeably diminished. This was presumably due to quenching by radicals generated during the photodegradation of the PAG. Following the soft bake, however, PL was fully restored. The pattern was revealed by gentle agitation of the substrate in a developing solvent such toluene or THF for roughly 30 s.

Förster Energy Transfer in Patterned Films. In an attempt to alter the PL emission of patterned substrates to include all three primary colors, dopants suitable for efficient Förster energy transfer were added to PSF resist solutions prior to spin-casting. The use of dopants to change emission wavelength is well documented and has been exploited in OLEDs based on sublimed molecular materials.[33−36] To a lesser extent, this approach has also been used in conjugated-polymer systems.[37] Figure 5a shows that following photopatterning and development, efficient energy transfer was observed to occur between the cross-linked host polymer and the added ~1 wt % of coumarin 540A (C540A, λ_{em} = 532 nm) or tetraphenylporphrin (TPP, λ_{em} = 635 nm). The result, as imaged using confocal fluorescence microscopy, is RGB patterns which demonstrate efficient single-step Förster transfer from blue to red or green emitters. The use of TPP allows an exceptionally large shift using a single-step transfer to obtain a

dx.doi.org/10.1021/am4025406 | ACS Appl. Mater. Interfaces 2014, 6, 83−93

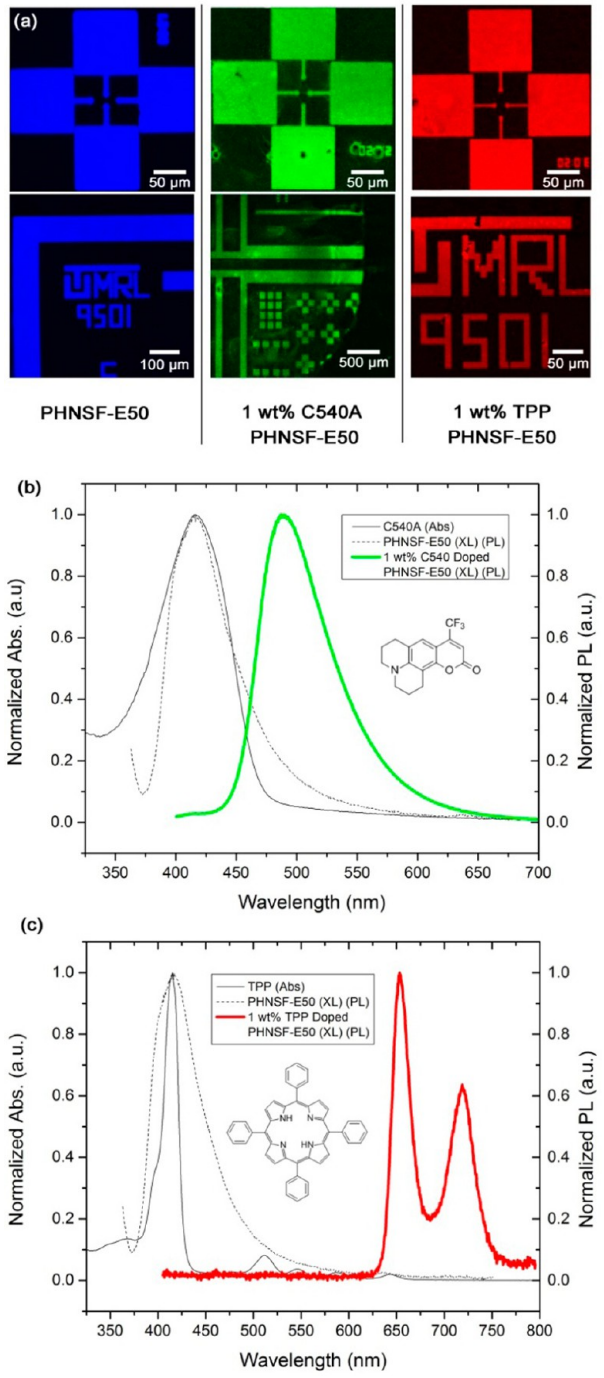

Figure 5. (a) Three confocal fluorescence microscope images of patterned substrates ranging in emission color from blue (neat PHNSF-E50), green (1 wt % C540A), and red (1 wt % TPP). (b) Normalized fluorescence spectra (λ_{ex} = 365 nm) taken of C540A doped patterned films. (c) Normalized fluorescence spectra (λ_{ex} = 365 nm) taken of TPP doped patterned films. Note that in both spectra there is complete suppression of the polymer emission in host/dopant systems.

saturated red emission. This is due mainly to the existence of a strongly blue absorbing Soret band which couples to a narrow Q-band red emission peak.[38] Figure 5c shows the photoluminescence spectra for cross-linked films of polymer PHNSF-E50 (**1**) neat and films doped with 1 wt % of TPP. The CIE coordinates corresponding to this host/dye system are x = 0.5694 and y = 0.2972. It is clear that even at low concentrations, the spectrum is dominated by the PL of TPP, which has a characteristic set of narrow peaks at 653 and 714 nm. Furthermore there is no apparent emission emanating from **1**. Referring to Figure 4 and the PL spectra of both polymers **1** and **2**, the emission maximum for these materials is 410 nm. This overlaps perfectly with the absorption of TPP (at 418 nm), hence efficient Förster energy transfer was anticipated.[39]

Analogously, the significantly broader absorption of C540A centers on 423 nm and fully overlaps with the emission of the host polymer and complete energy transfer to the dye is observed even at low loadings. Figure 5b shows the PL of the C540A doped films of polymer **1**. Excitation at 365 nm results in green emission (λ = 530 nm) with no observable blue emission from the polymer. The CIE coordinates corresponding to this host/dye system are x = 0.1919 and iy = 0.4108).

For each dopant/host system the Förster radius (R_0) was calculated as an initial indicator of ideal dye concentration. R_0 is defined as the minimum distance separating donor and acceptor compounds such that intermolecular energy transfer and donor fluorescence are equally probable relaxation channels. Radii for both TPP and C540A were calculated using the following equation:[35]

$$(R_0)^6 = \frac{0.5291K^2}{N_A n^4} T \tag{1.0}$$

where K^2 = 0.66 for randomly oriented dipoles, N_A is Avogadro's number, n is the refractive index of the material (n_{PSF} = 1.75 as measured by ellipsometry), and T is known as the overlap integral of the normalized PL of the host material and the spectral extinction coefficient plotted against wavelength in wavenumbers and is defined by eq 1.1[35]

$$T = \int_0^\infty F_D(\nu)\varepsilon_A(\nu)\nu^4 d\nu \tag{1.1}$$

where F_D is the normalized PL spectrum of the donor as a function of wavelength, ε_A is the decadic extinction coefficient of the acceptor (in $M^{-1}cm^{-1}$), and ν is wavelength in centimeters. Reference absorption spectra taken of TPP and C540A used in the calculation of T can be found in the Supporting Information. The values of R_0 calculated for TPP and C540A in polymers **1** or **2** are 9.4 and 7.4 nm, respectively. These values are notably larger than previous estimates of R_0 for TPP in poly(9,9-dioctylfluorene) (PFO) films because of greater host/dopant spectral overlap. On the basis of theory, we would expect a minimum dye concentration of 0.025 and 0.03 wt % of TPP and C540A respectively to induce 50% of excited state electrons to decay to the ground state via intermolecular energy transfer. This is well within the concentration regime wherein minimal phase segregation is observed. If we plot the absolute quantum yields (AQY) of both dye/host systems as a function of dye loading (expressed in wt %), we observe a trend in energy transfer efficacy which closely correlates with the calculated value of intermolecular dye spacings.

Figure 6a plots the AQY of different compositions of the TPP/PHNSF-E50 within the range of 0.025−1.5 wt % TPP. Beginning at 0.025 wt % TPP, the total quantum yield of the system (48.2%) has contributions from both PHNSF-E50 and TPP of 43.3% and 4.9% respectively. Keeping in mind the 86% AQY for films of PHNSF-E50 is a factor of 8.6 higher than the 10% AQY of TPP doped films of PMMA, a dye concentration of 0.025 wt % corresponds to the approximate Förster Radius.

dx.doi.org/10.1021/am4025406 | ACS Appl. Mater. Interfaces 2014, 6, 83−93

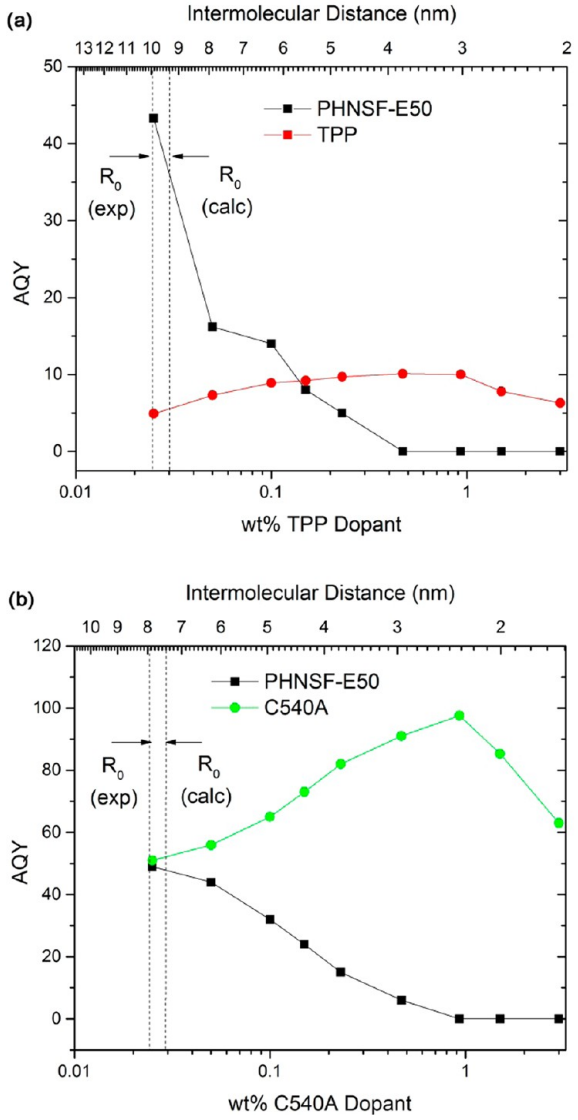

Figure 6. Plot of AQY as a function of (a) TPP and (b) C540A dye loading over the range of 0.025−3 wt % in thin films of PHNSF-E50. The top *x*-axis corresponds to the approximate intermolecular distance between dye molecules. Maximum energy transfer is observed for loadings of ∼1 wt % where no emissions from the polymer host are observed. The dashed line indicates the calculated R_0 determined by eq 1.0 and 1.1 and experimentally determined values of R_0. Similar results were obtained for thin films of PHCySF-E50.

Assuming each molecule of TPP occupies a spherical volume of $(4/3)\pi l^3$, the intermolecular distance l is calculated to be 9.8 nm. This discrepancy with the theoretical value of 9.4 nm, as previously rationalized in the case of PFO, is due to the extended conjugation of the polymer backbone and hence the wave function of an excited state is not limited to a single repeat unit. This extends the range of dipole−dipole interaction and increases the Förster Radius.[35]

Following the increase of TPP concentration to 1 wt %, the AQY has only a single contribution from TPP at a maximum value of 10%. This can only be the result of near quantitative transfer of energy from the excited state of PHNSF-E50 to TPP while irradiated with 365 nm light. Note that increasing TPP concentration results in the eventual decline of AQY. It is safe to posit that reduced TPP intermolecular distance increases the probably of self-quenching via nonradiative pathways.[35]

The AQY of C540A is significantly higher (82% in 1.5 wt % PMMA) than TPP, yet the calculated overlap integral is still comparable and consequently, a similar Förster radius and dye concentration is expected for complete energy transfer. Because the AQY of both PHNSF-E50 and C540A are similar, we can conclude from Figure 6b that the concentration of C540A corresponding to the Förster radius is 0.03 wt %. Increasing the concentration of C540A to 1.2 wt % completely suppresses any emission from PHNSF-E50 and the AQY approaches the expected value 80%. Analogous to TPP, an increase in C540A concentration above 2 wt % resulted in a noticeable decline in AQY.

The ability of PSF to act as host is potentially important for applications since it allows a single material to be used as a blue light emitter, as a host for green emission dyes, and as a host for a red emission dye. These results demonstrate a unique potential for PSF to assist in the simple construction of ultra high resolution multicolour displays. Of course, covalently bonding dyes to the backbone would eliminate the risk of leaching dopant during the development stage, but thus far leach rates we observed are slow enough such that desired spectral shifts were obtained. That said, we have already had considerable success in an initial attempt to covalently bind dopant emitters through emerging "click" chemistry methods based on tetrazine derivatives.[40−43] Unlike copper catalyzed azide/alkyne cycloadditions, tetrazines react rapidly with norbornene moieties at room temperature without need of metal catalyst. This work will appear in a future publication.

Electroluminescent Device With Cross-linked Emissive Layer. Energy levels of polymer (5) was previously determined by cyclic voltammetry (CV).[19] It was found that HOMO/LUMO energy levels (5.7 and 2.7 eV, respectively) reside slightly lower than most reported for PFO and found suitable for OLED applications. We estimate the energy levels of the corresponding polymers (1) are the same (given no changes occur to the conjugated silafluorene backbone during epoxidation). Light emitting devices were constructed in a N_2 filled glovebox on O_2 plasma treated ITO on glass. We employed a simple trilayer design using PEDOT:PSS as the hole injection layer (∼10 nm) as well as a thin hole transport layer consisting of poly[*N*,*N*′-bis(4-butylphenyl)-*N*,*N*′-bis-(phenyl)-benzidine] (poly-TPD) (∼ 20 nm). A contiguous 80 nm emissive layer consisting of PHNSF-E50 was deposited by spin-casting from an 8 mg/mL polymer solution in toluene. The solution also contains roughly 4 mol % (with respect to epoxide) of the PAG DtBPI-PF_6 (see Photolithography Methods). To cross-link the emissive layer, the device was briefly flooded with 365 nm UV light from a collimated LED source (190 mW, Thor Laboratories) and baked at 90 °C for 30s. Residual unreacted polymer (if any) and PAG residues where removed by washing the layers with toluene. Remaining wash solvent was eliminated by placing the device in the glovebox antechamber and evacuating for 30 min. The device was completed following the evaporation of a low work function metal under low pressure onto a known area defined by a shadow mask. A calcium cathode, which best matches the LUMO energy of 2.7 eV, was found to yield the best performing devices. Figure 7a illustrates the device architecture and energy levels of the respective layers. A photograph of an encapsulated functional device operating at 9 V is shown in figure 7b alongside its respective electroluminescence spectra. The EL is similar to the cross-linked thin film PL spectrum of **1** and consists of a single peak centered at 410 nm. The full width

dx.doi.org/10.1021/am4025406 | ACS Appl. Mater. Interfaces 2014, 6, 83−93

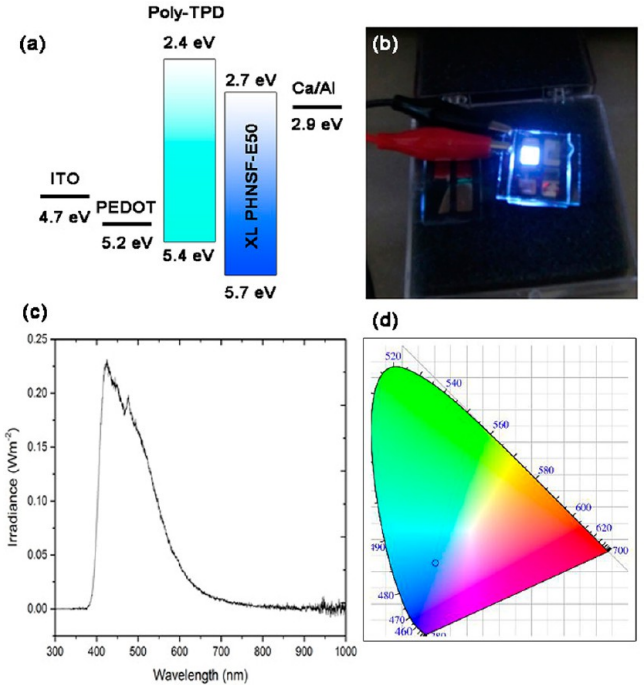

Figure 7. (a) Illustration of LED architecture indicating respective energy levels of layers. (b) Photograph of a device under 9 V operation. (c) Plot of electroluminescence spectra obtained from device operating at 9 V. (d) CIE color map highlighting the position of the blue-violet OLED EL.

at half-maximum (fwhm) of the EL peak is 166 nm. Figure 7d shows the location of the device's blue-violet emission on the CIE color map. Its CIE coordinates are x = 0.2042 and y = 0.2319.

Performance data obtained for our champion device is presented in Figures 8 and 9. Beginning with the $I-V-L$ curve in Figure 8, we observe the turn on voltage to be roughly 5 V. The device was operated up to 10 V and reached a maximum current density of 60 mA/cm^2. The maximum luminance

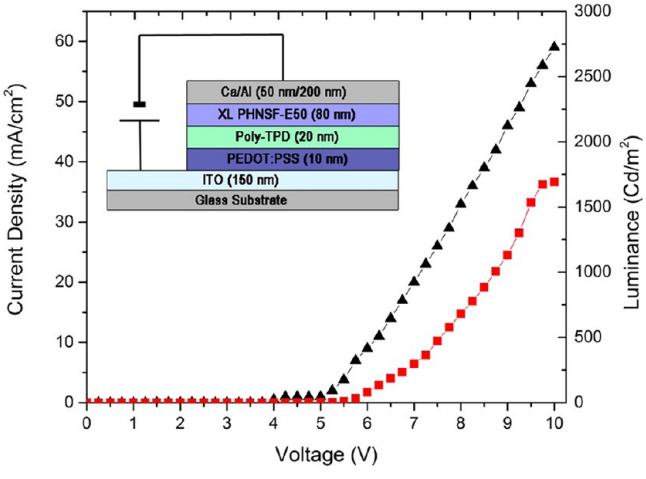

Figure 8. Cross-linked PHNSF-E50 device characteristics: Luminance (solid squares) and current density (solid triangles) vs bias voltage. The luminance reaches its maximum at 1690 Cd/m^2. The onset voltage was ~5 V. The inset show the device architecture ITO/PEDOT:PSS (10 nm)/poly-TPD (20 nm)/XL-PHNSF-E50 (80 nm)/Ca/Al (50 nm/200 nm).

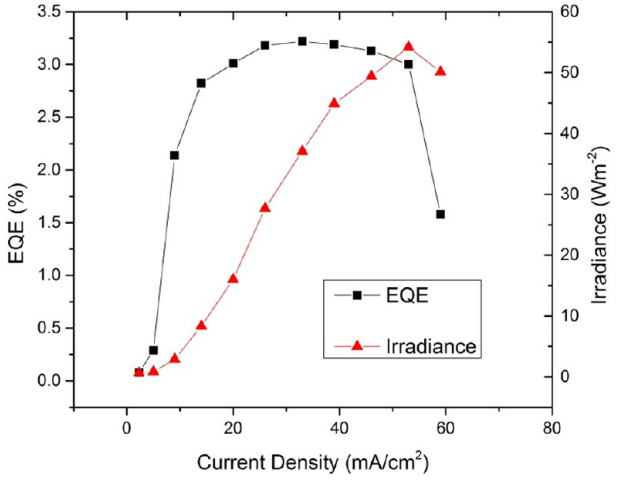

Figure 9. Plot of EQE and irradiance as a function of current density. Note the maximum efficiency achieved was 3.2% at 33 mA/cm^2 (corresponding to a power efficiency of 1.62 Im/W).

measured for the device was 1690 Cd/m^2 at 10 V operation. Compared to current state-of-the-art blue emitting polymer OLEDs,[43] which can achieve maximum luminescence of 10500 Cd/m^2, our device performs moderately but represents an improvement over more closely related OLEDs based on photo-cross-linked emissive layers such as those reported by Carter et al. which can obtain a maximum luminance of 150 Cd/m^2.[11] Our device brightness is also comparable to the blue emitting cross-linked OLED devices reported by Meerholtz et al.[15] Figure 9 show the maximum irradiance of our device was 54 W/m^2 at a current density of 53 mA/cm^2. The maximum external quantum efficiency of the device is 3.2% when operating at 33 mA/cm^2 and corresponds to a maximum power efficiency of 1.62 Im/W.

DFB Laser With Cross-linked Emissive Layer. In addition to electroluminescent devices, we explored the performance of cross-linked films of PHNSF-E50 and PHCySF-E50 as gain medium in thin film distributed feedback (DFB) lasers. The strong absorption and broad emission of conjugated polymers are features which make these materials ideal candidates for solid state lasers in the visible spectral range. There are many resonator configurations pre-existing in the literature including microcavities, microdisk, microtoroidal, microcone lasers in addition to distributed feedback structures.[44] DFBs have gained particular attention because of their relatively simple fabrication from polymer solutions and their propensity for low threshold operation in combination with a well-defined output beam.

Prior to building an actual laser, we examined the photophysical properties of our materials through the use of pump–probe measurements (at a repetition rate of 1 kHz and pulse duration of ~200 fs).[45] Figure 10 presents evidence of gain in PHCySF-E50 which has been cross-linked after being spin-cast onto a glass substrate. The ordinate of Figure 10 is the change in the optical density (OD) at the probe wavelength so a coherence peak (representing an increase in absorption of the probe pulse) is due to further excitation of the excited carriers (by the pump) when pump photons (388 nm) and probe photons (489 nm) reach the sample at exactly the same time. Pump-induced absorption, however, becomes negative after several picoseconds when carriers have relaxed to luminescent energy states. Incoming probe photons cause carriers to

dx.doi.org/10.1021/am4025406 | ACS Appl. Mater. Interfaces 2014, 6, 83–93

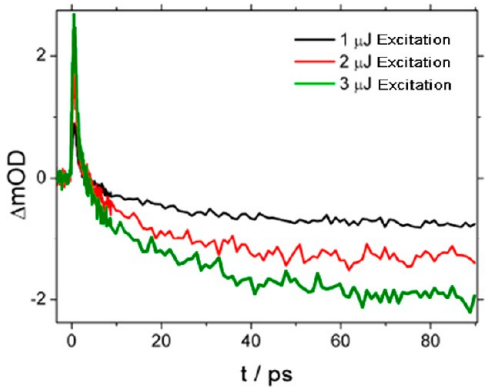

Figure 10. Measurement of optical gain in cross-linked films of PHCySF-E50 determined by time-resolved pump−probe (388/489 nm).

recombine due to stimulated emission (SE). SE counterbalances the absorption of the probe pulse and is perceived as a negative absorption (e.g., a negative change in optical density).

Figure 11 plots the fluorescence lifetimes (τ) of the same PHCySF-E50 cross-linked film in addition to a noncross-linked

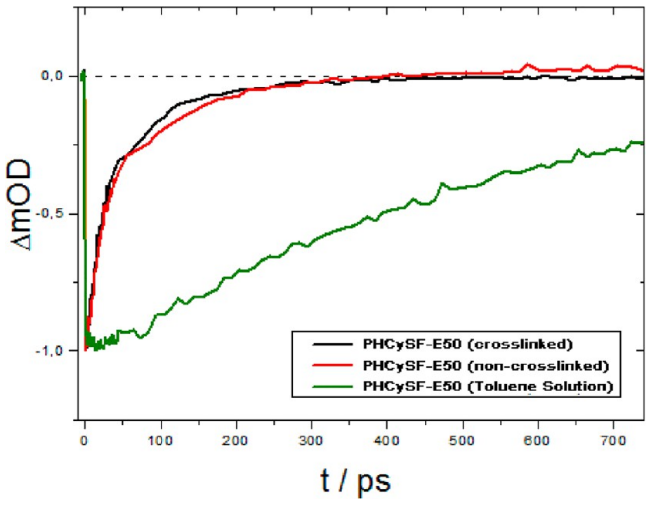

Figure 11. Plot of fluorescent lifetime of in cross-linked films of PHCySF-E50, noncross-linked films of PHCySF-E50, and a dilute solution in toluene (pump at 360 nm, probe at 440 nm).

film and a solution of the polymer in toluene. The fluorescence decay in the films is on the order of a few hundred picoseconds, which is consistent with the decay time of the stimulated-emission signal. It is clear from Figure 11 that fluorescence is significantly longer lived in solution where chain separation is significant and quenching is reduced.

The inset of Figure 12 illustrates the structure of the polymer DFB laser produced in this study. Note that there is a periodic modulation in the refractive index which results in diffractive feedback along one axis in the waveguide plane. As such, lasers were constructed by spin-casting a thin polymer layer (~100 nm) from solution on corrugated silica structures produced by reactive ion etching (RIE) of thermally grown SiO_2 on silicon wafers. The gratings had a modulation depth of 100 nm and a grating periodicity of 200 nm with a duty cycle of 0.5. The system was optically pumped with a Q-switched frequency-tripled neodymium-doped yttrium ortho-vanadate ($Nd:YVO_4$) laser (AOT Inc.) with a wavelength of 355 nm and pulse

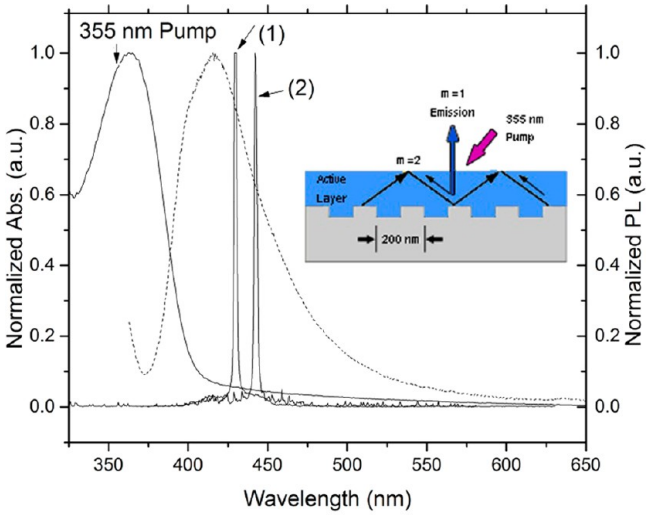

Figure 12. Plot of second-order laser emissions from cross-linked films of PHNSF-E50 and PHCySF-E50 on corrugated silica substrates (Λ = 200 nm). (Inset illustrates the structure of the laser and the measurement geometry).

duration of 0.5 ns. To prevent the photooxidation of the organic material, the sample was characterized in a vacuum chamber (<5 × 10^{-5} mbar). Using an automated precision stage, the sample chamber is able to move in both directions within the plane orthogonal to the pump beam. Upon excitation, light propagating in a waveguide mode of the organic film is scattered by the periodic corrugations.[46−49] A wave is formed from scattered light from each corrugation combining coherently and propagating in a new direction. For a given period of the corrugation, the wavelength of light that will be diffracted is that which satisfies the Bragg condition

$$m\lambda = 2n_{\text{eff}}\Lambda \quad (1.2)$$

Here, λ is the wavelength of the light, Λ is the period of the structure, and im is an integer that represents the order of the diffraction. n_{eff} is the effective refractive index of the waveguide. Given Λ = 200 nm in our system, second-order feedback (m = 2) was measured from the surface of the film perpendicular to the plane of the waveguide.

The reflected wavelength is expected to equal $n_{\text{eff}}\Lambda$. While second-order structures can provide a surface-emitted output, it comes at the cost of higher oscillator thresholds given that the out-coupled laser power represents a loss mechanism. Figure 12 shows the laser output of cross-linked films of PHNSF-E50 (1) and PHCySF-E50 (2). Slightly higher wavelength of the polymer (2) laser is due to a difference in organic layer thickness which impacts the value of n_{eff}.

CONCLUSION

We have demonstrated a unique method of preparing photopatternable blue emitting conjugated polymers which are functionalized with pendent epoxide side groups. Postpolymerization epoxidation of cyclohexenyl and norbornenyl was accomplished using a well-known oxidant, m-CPBA, and a straightforward method that yields product within minutes. We noted that due to the increased ring strain of norbornenyl moieties, the extent of epoxidation was more easily controlled and conversion could be greater than 80%. Solutions of polymer suitable for spin-casting into contiguous transparent films were made in toluene. Adding an iodonium based PAG

dx.doi.org/10.1021/am4025406 | ACS Appl. Mater. Interfaces 2014, 6, 83−93

allowed films to be patterned with resolution <10 μm following UV light exposure through a shadow mask. We believe polymers **1** and **2** have qualities superlative to the existing art given the minimal synthesis time required for our nickel catalyzed polymerization and signal step epoxidation while matching the performance of polymers produced by the lengthier Suzuki coupling polymerizations and more synthetically complex oxetane functionalization.

In future work, we will illustrate that the cycloalkene moieties purposefully left unreacted during epoxidation, are excellent functionalities through which further side chain modifications can be made, specifically the tethering of auxiliary chromophores for full spectrum emission tuning in pixelated substrates. This will enable us to expand on our existing demonstration of a 3% EQE cross-linked blue emitting OLED and generate a patterned substrate with separate RGB electroluminescence. An emerging "click" chemistry method utilizing 2 + 4 cycloaddition of tetrazine derivatives represents a potentially revolutionary means of tailoring conjugate polymer emission. The catalyst free reaction is rapid at room temperature and the covalently bound chromophores would be prevented from phase segregating in thin films.

Our observation of amplified spontaneous emission from cross-linked polymer films is the first demonstration of this important quality in photopatternable PSF. In future work, we will expand upon the concept of patterning cross-linkable gain medium into resonators. Specifically, we will demonstrate how advanced lithography technologies, such as two photon direct laser writing, can be used to print 3D waveguiding structures. Potential structures could include toroids which have extremely high Q factor ($>10^7$) and could potentially reduce lasing thresholds to the limits of electrical excitation.

EXPERIMENTAL SECTION

Chemicals and solvents were purchased from TCI America and Sigma Aldrich and used without need for further purification. NMR was performed on a 400 MHz Bruker Avance III Spectrometer. Thin film absorption and photoluminescence spectra were recorded using a Perkin-Elmer 900 UV−vis Spectrometer and a Perkin-Elmer LS-50B Luminescence Spectrophotometer. Polymer quantum efficiencies were calculated through the use of an integrating sphere using a focused 365 nm LED (190 mW, Thor Laboratories) as the excitation source and an Ocean Optics Maya Pro CCD optical fiber spectrometer. High resolution patterning of polymer films was done using a Karl Suss M6 mask aligner in a clean room facility. Laser spectra were recorded using a fiber coupled CCD camera and excitation was provided by Q-switched frequency-tripled neodymium-doped yttrium orthovanadate ($Nd:YVO_4$) laser (AOT-YVO-20QSP, Advanced Optical Technology Ltd.) with a wavelength of 355 nm. Gratings used for thin film laser substrates where produced using e-beam lithography and RIE of a thermally grown oxide layer on Silicon wafers. In the measurement of stimulated emission (SE), a Clark 2210 laser system was used with a 1 kHz repetition rate at 775 nm. Thin films on glass were irradiated with a 1−3 μJ/pulse collimated 3 mm beam with pulse durations of 200 fs. Pump and probe wavelengths were derived from the second harmonic of the Clark output (388 nm) and 489 nm (noncollinar optical parametric amplification: NOPA) respectively. Measurements of fluorescence lifetimes used a 360 nm pump and a 440 nm probe (sum frequency mixing of the fundamental and appropriate NOPA wavelength) with a 150 fs pulse duration at 0.46 μJ/pump pulse. $I-V-L$ characteristics of fabricated OLEDs were measured using a Keithley 2400 SourceMeter and a calibrated integrating sphere coupled to a fiber spectrometer and a silicon photodiode detector.

Prilezhaev Epoxidation of Polymers PHCySF (4) and PHNSF (5). The synthesis of 2,7-dibromo-3,6-dimethoxy-9-hexyl-9-[2-(cyclohex-3-en-1-yl)ethyl]silafluorene (HCySF) and 2,7-dibromo-3,6-dimethoxy-9-hexyl-9-[2-(bicyclohept-5-en-2-yl)ethyl]silafluorene (HNSF) monomers and the procedure for their polymerization to PHCySF (**4**) and PHNSF (**5**) has been published by our group previously.[19] Details for synthesizing both monomer and polymer starting materials is provided in the Supporting Information along with characteristic spectral data. The following procedure for the selective epoxidation of cyclohexenyl and norbornenyl moieties (via the Prilezhaev reaction) is applicable to both polymers **4** and **5**.

*Prilezhaev Epoxidation of PHNSF (**5**).* Beginning with PHNSF (50 kg/mol, PDI = 1.8, see Supporting Information for synthesis details), the selective epoxidation of 50% norbornenyl side groups is accomplished by dissolving 200 mg of polymer (0.46 mmol norbornenyl moieties) in 11 mL of toluene in a large screw top vial. The solution was cooled in an ice bath until the temperature fell below 5 °C. In a separate vial, a solution of 72% m-chloroperoxybenzoic acid (m-CPBA) was prepared in DCM (53 mg/mL, 0.25 M). mCPBA solution was also cooled in an ice bath. For a 50% epoxidation, 720 μL of the cooled m-CPBA solution was slowly added dropwise to a rapidly stirring polymer solution. The reaction was continuously stirred at low temperature for a period of 10−15 min before removing from the ice bath and precipitating the product via the addition of hexanes. The product was allowed to settle (or collected using a centrifuge) and the solvent was removed prior to drying the white solid in vacuo. To remove residue of m-CPBA, the product was precipitated twice from a concentrated THF solution into methanol before finally being dissolved in toluene to make a 32 mg/mL solution. The reaction yield is quantitative excluding losses from material transfer during purification. (PHNSF-E50) (**1**): ^{1}H NMR (CD_2Cl_2, 400 MHz) (ppm) 7.45 (s, 2H), 7.46 (s, 2H), 6.12−5.81 (m, 1H), 3.91 (s, 6H), 2.71 (d, 1H), 2.60−0.39 (m, 22H). (PHCySF-E50) (**2**): ^{1}H NMR (CD_2Cl_2, 400 MHz) (ppm) 7.47 (s, 2H), 7.42 (s, 2H), 5.55 (s, 1H), 3.91 (s, 6H), 3.01 (s, 1H), 1.91−0.77 (m, 24H).

Photopatterning of Polymer Films. The 16 mg/mL toluene polymer solutions (prepared in the previous section) were mixed in equal parts with a 0.5 mg/mL toluene solution of bis(4-*tert*-butylphenyl)iodonium hexafluorophosphate (DtBPI-PF_6). The resultant mixture was filtered through 0.22 μm PTFE syringe filters prior to use. Thin, contiguous films (80−100 nm) of polymers **1** and **2** were formed by spin-casting at rates of 1000 rpm for 2 min. Without a soft bake, substrates were photopatterned using a chromium-on-quartz shadow mask with a printed test pattern and the 365 nm I-line of a low pressure mercury arc lamp used in a Karl Suss M4 mask aligner. A N_2 stream was used to blanket the substrate from air during the exposure to prevent photooxidation. Samples were removed from the maskaligner and soft baked at 90 °C for 30 s under a nitrogen blanket. Once cooled, patterns were developed by submerging the substrates in toluene and lightly agitating the container. Removal of noncross-linked material normally occurs within 30 s. The films were dried with a N_2 gun and analyzed with respect to PL via confocal microscope. In cases where Förster dopants were used, the above procedure was followed with the addition of the correct amount of either C540A or TPP added to the polymer solution prior to spin-casting.

Electroluminescent Device Fabrication. OLEDs were prepared using prepatterned ITO substrates (7 ohm/sqr, Visiontek Inc.), which were cleaned using O_2 plasma for a period of 5 min. PEDOT:PSS (AL4083) was diluted (1:1 v/v) with distilled water prior to spin-casting at 3000 rpm for 2 min (acceleration was set to 1000 rpm/s). The substrates were transferred to a N_2 filled glovebox and dried by heating at 110 °C for 30 min on a hot plate. All subsequent processing was done under N_2. Once cooled, a hole injection layer (HIL) was deposited by spin-casting a 10 mg/mL chlorobenzene poly-TPD (American Dye Source) solution at 2000 rpm for 2 min (acceleration = 1000 rpm/s). The HIL layer was dried by baking substrate at 150 °C for 30 min. Once cooled, the emissive polymer layer (either **1** or **2**) was deposited by spincasting an 8 mg/mL toluene solution (containing ∼4 mol % DtBPI-PF_6) at 1000 rpm for 2 min (acceleration =1000 rpm/s). Without soft bake, the substrate was placed under a 365 nm UV LED (190 mW, Thor Laboratories) and exposed for 5 s. Cross-linking was completed by a 90 °C soft bake for

dx.doi.org/10.1021/am4025406 | ACS Appl. Mater. Interfaces 2014, 6, 83−93

30 s. Residual amounts of noncross-linked material and PAG residues were removed by submerging the substrate in toluene within a large screw-top vial. The substrate was placed in the glovebox antechamber dried under vacuum for a period of 30 min prior to depositing a Ca/Al cathode. The optimal calcium layer thickness was 50 nm (deposited at a rate of 0.8 Å/s). The aluminum layer thickness was 200 nm (deposited at a rate of 1 Å/s). I–V-L device characteristics were measured following the encapsulation of the OLEDs to protect them from degradation.

■ ASSOCIATED CONTENT

Supporting Information

Detailed synthetic protocols for producing HCySF and HNSF monomers and methods and higher resolution images of patterned substrates, as well as reference absorption spectra for C540A and TPP. This material is available free of charge via the Internet at http://pubs.acs.org.

■ AUTHOR INFORMATION

Corresponding Author

*E-mail: gozin@chem.utoronto.ca.

Notes

The authors declare no competing financial interest.

■ ACKNOWLEDGMENTS

G.O. is Government of Canada Research Chair in Materials Chemistry and Nanochemistry. J.J.M. is an NSERC Graduate Fellow. Both are deeply indebted to the Natural Sciences and Engineering Research Council for strong and sustained support of their work. F.M.-F. acknowledges generous support by the Karlsruhe School of Optics & Photonics (KSOP). T.J.A.W. and A.-N.U. acknowledge financial support provided by the Deutsche Forschungsgemeinschaft (DFG), the State of Baden-Württemberg and the Karlsruhe Institute of Technology (KIT) through the DFG-Center for Functional Nanostructures (CFN) and the Fonds der Chemischen Industrie,

■ REFERENCES

(1) Bardsley, J. N. *IEEE J. Sel. Top. Quantum Electron.* **2004**, *10*, 3–9.
(2) Shinar, J.; Shinar, R. *J. Phys. D: Appl. Phys.* **2008**, *41*, 133001/1–133001/26.
(3) Menard, E.; Meitl, M. A.; Sun, Y.; Park, J.-U.; Shir, D. J.-L.; Nam, Y.-S.; Jeon, S.; Rogers, J. A. *Chem. Rev.* **2007**, *107*, 1117–1160.
(4) Forrest, S. R.; Thompson, M. E. *Chem. Rev.* **2007**, *107*, 923–925.
(5) Feehery, W. F.; Flattery, D.; Herron, N.; Lang, C.; O'Regan, M. *Inf. Disp.* **2007**, *23* (10), 28–33.
(6) Chesterfield, R.; Johnson, A.; Lang, C.; Stainer, M.; Ziebarth, J. *Inf. Disp.* **2011**, *27* (1), 24–30.
(7) Arias, A. C.; MacKenzie, J. D.; McCulloch, I.; Rivnay, J.; Salleo, A. *Chem. Rev.* **2010**, *110*, 3–24.
(8) Flattery, D. K.; Curtis, C. R.; Fincher, R.; LeCloux, D. L.; O'Regan, M. B.; Richard, J. S. *Inf. Disp.* **2011**, *27* (10), 8–13.
(9) Yagi, I.; Hirai, N.; Miyamoto, Y.; Noda, M.; Imaoka, A.; Yoneya, N.; Nomoto, K.; Kasahara, J.; Yumoto, A.; Urabe, T. *J. Soc. Inf. Disp.* **2008**, *16*, 15–20.
(10) Muller, C. D.; Falcou, A.; Reckefuss, N.; Rojahn, M.; Wiederhirn, V.; Rudati, P.; Frohne, H.; Nuyken, O.; Becker, H.; Meerholz, K. *Nature* **2003**, *421*, 829–833.
(11) Davis, A. R.; Maegerlein, J. A.; Carter, K. R. *J. Am. Chem. Soc.* **2011**, *133*, 20546–20551.
(12) Ventsch, F.; Gather, M. C.; Meerholz, K. *Org. Electron.* **2010**, *11*, 57–61.
(13) Wallikewitz, B. H.; de la Rosa, M.; Kremer, J. H.-W. M.; Hertel, D.; Meerholz, K. *Adv. Mater.* **2010**, *22*, 531–534.
(14) Gather, M. C.; Kronenberg, N. M.; Meerholz, K. *Adv. Mater.* **2010**, *22*, 4634–4638.
(15) Gather, M. C.; Koehnen, A.; Falcou, A.; Becker, H.; Meerholz, K. *Adv. Fuct. Mater.* **2007**, *17*, 191–200.
(16) Zacharias, P.; Gather, M. C.; Rojahn, M.; Nuyken, O.; Meerholz, K. *Angew. Chem., Int. Ed.* **2007**, *46*, 4388–4392.
(17) Mack, C. *Fundamental Principles of Optical Lithography: The Science of Microfabrication*; John Wiley & Sons Ltd., Wiley-Interscience: Chichester, U.K., 2011; p 257.
(18) Levinson, H., J. *Principles Of Lithography*; SPIE Press: Bellingham, Washington, 2005; p 80.
(19) McDowell, J. J.; Schick, I.; Price, A.; Faulkner, D.; Ozin, G. A. *Macromolecules* **2013**, *46* (17), 6794–6805, DOI: 10.1021/ma401346y.
(20) Rabe, T.; Hoping, M.; Schneider, D.; Becker, E.; Johannes, H.-H.; Kowalsky, W.; Weimann, T.; Wang, J.; Hinze, P.; Nehls, B. S.; Scherf, U.; Farrell, T.; Riedl, T. *Adv. Funct. Mater.* **2005**, *15*, 1188–1192.
(21) Anni, M.; Alemanno, M. *Phys. Rev. B: Condens. Matter Mater. Phys.* **2008**, *78*, 233102/1–233102/4.
(22) Rothe, C.; Galbrecht, F.; Scherf, U.; Monkman, A. *Adv. Mater.* **2006**, *18*, 2137–2140.
(23) Anni, M.; Caruso, M. E.; Lattante, S.; Cingolani, R. *J. Chem. Phys.* **2006**, *124*, 134707/1–134707/7.
(24) Khan, A. L. T.; Sreearunothai, P.; Herz, L. M.; Banach, M. J.; Kohler, A. *Phys. Rev. B: Condens. Matter Mater. Phys.* **2004**, *69*, 085201/1–085201/8.
(25) Vogel, A. I.; Tatchell, A. R.; Furnis, B. S.; Hannaford, A. J.; Smith, P. W. G. *Vogel's Textbook of Practical Organic Chemistry*, 5th ed.; Prentice Hall, Longman Group UK: Edinburgh Gate, U.K., 1996; p 1134.
(26) Smith, M. B.; March, J. *March's Advanced Organic Chemistry: Reactions, Mechanisms, and Structure*, 6th ed.; John Wiley & Sons Eds., Wiley-Interscience: Hoboken, NJ, 2007; p 1171.
(27) Shea, K. J.; Kim, J. S. *J. Am. Chem. Soc.* **1992**, *114*, 3044–3951.
(28) Agarwal, D. D.; Jain, R.; Chakravorty, A.; Rastogi, R. *Polyhedron* **1992**, *11*, 463–467.
(29) Mei, C.; Ding, J.; Yao, B.; Cheng, Y.; Xie, Z.; Geng, Y.; Wang, L. *J. Polym. Sci., Part A: Polym. Chem.* **2007**, *45*, 1746–1757.
(30) Shao, S.; Ding, J.; Wang, L.; Jing, X.; Wang, F. *J. Am. Chem. Soc.* **2012**, *134*, 20290–20293.
(31) Tan, H.; Yu, J.; Wang, Y.; Li, J.; Cui, J.; Luo, J.; Shi, D.; Chen, K.; Liu, Y.; Nie, K.; Zhu, W. *J. Polym. Sci., Part A: Polym. Chem.* **2011**, *50*, 149–155.
(32) Park, M.-J.; Kwak, J.; Lee, J.; Jung, I. H.; Kong, H.; Lee, C.; Hwang, D.-H.; Shim, H.-K. *Macromolecules* **2010**, *43*, 1379–1386.
(33) Cerullo, G.; Stagira, S.; Zavelani-Rossi, M.; De Silvestri, S.; Virgili, T.; Lidzey, D. G.; Bradley, D. D. C. *Chem. Phys. Lett.* **2001**, *335*, 27–33.
(34) Ego, C.; Marsitzky, D.; Becker, S.; Zhang, J.; Grimsdale, A. C.; Mullen, K.; MacKenzie, J. D.; Silva, C.; Friend, R. H. *J. Am. Chem. Soc.* **2003**, *125*, 437–443.
(35) Virgili, T.; Lidzey, D. G.; Bradley, D. C. C. *Adv. Mater.* **2000**, *12*, 58–62.
(36) Kaur, A.; Cazeca, M. J.; Sengupta, S. K.; Kumar, J.; Tripathy, S. K. *Synth. Met.* **2002**, *126*, 283–288.
(37) Gupta, R.; Stevenson, M.; Dogariu, A.; McGehee, M. D.; Park, J. Y.; Srdanov, V.; Heeger, A. J.; Wang, H. *Appl. Phys. Lett.* **1998**, *73*, 3492–1–3492/3.
(38) Shoustikov, A.; You, Y.; Burrows, P. E.; Thompson, M. E.; Forrest, S. R. *Synth. Met.* **1997**, *91*, 217–221.
(39) Sauer, M.; Hofkens, J.; Enderlein, J. *Handbook of Fluorescence Spectroscopy and Imaging: From Ensemble to Single Molecules*; John Wiley & Sons, Wiley-VCH Verlag GmbH & Co. KGaA: Weinheim, Germany, 2010; p 64.
(40) Clavier, G.; Audebert, P. *Chem. Rev.* **2010**, *110*, 3299–3314.
(41) Han, H.-S.; Devaraj, N. K.; Lee, J.; Hilderbrand, S. A.; Weissleder, R.; Bawendi, M. G. *J. Am. Chem. Soc.* **2010**, *132*, 7838–7839.
(42) Devaraj, N. K.; Weissleder, R.; Hilderbrand, S. A. *Bioconjugate Chem.* **2008**, *19*, 2297–2299.

(43) Nau, S.; Schulte, N.; Winkler, S.; Frisch, J.; Vollmer, A.; Koch, N.; Sax, S.; List, E. J. W. *Adv. Mater.* **2013**, *25*, 4420−4424.
(44) Samuel, I. D. W.; Turnbull, G. A. *Chem. Rev.* **2007**, *107*, 1272−1295.
(45) Wolf, T. J. A.; Fischer, J.; Wegener, M.; Unterreiner, A.-N. *Opt. Lett.* **2011**, *36*, 3188−3190.
(46) McGehee, M. D.; Diaz-Garcia, M. A.; Hide, F.; Gupta, R.; Miller, E. K.; Moses, D.; Heeger, A. J. *Appl. Phys. Lett.* **1998**, *72*, 1536/1−1536/3.
(47) Turnbull, G. A.; Andrew, P.; Jory, M. J.; Barnes, W. L.; Samuel, I. D. W. *Phys. Rev. [Sect.] B* **2001**, *64*, 125122/1−125122/6.
(48) Kallinger, C.; Hilmer, M.; Haugeneder, A.; Perner, M.; Spirkl, W.; Lemmer, U.; Feldmann, J.; Scherf, U.; Mullen, K.; Gombert, A.; Wittwer, V. *Adv. Mater.* **1998**, *10*, 920−923.
(49) Riedl, T.; Rabe, T.; Johannes, H.-H.; Kowalsky, W.; Wang, J.; Weimann, T.; Hinze, P.; Nehls, B.; Farrell, T.; Scherf, U. *Appl. Phys. Lett.* **2006**, *88*, 241116/1−241116/3.